Journal of Applied Polymer Science

The Effect of Morphology on the Flame-Retardant Behaviors of Melamine Cyanurate in PA6 Composites

Shuo Tang, Li-jun Qian, Yong Qiu, Nan Sun
Department of Materials Science & Engineering, Beijing Technology and Business University, Beijing 100048, People's Republic of China
Correspondence to: L. Qian (E-mail: augusqian@163.com)

ABSTRACT: Three types of melamine cyanurate (MCA) with micrometer-size sphere-like, micrometer-scale rod-like, and nanometer-scale flake-like morphologies were synthesized by changing the chemical circumstances of the reactions. The microcosmic morphologies of MCA were characterized via scanning electron microscopy and X-ray diffraction. After the MCAs with different morphologies were incorporated into polyamide 6 (PA6), the flame-retardant properties of the MCA/PA6 composites were investigated using the limited oxygen index (LOI), UL94, and cone calorimeter tests. The MCA/PA6 composites with nanometer-scale flake-like MCA obtained an LOI value of 29.5% and a UL94 V-0 rating, which were higher than those with micrometer-size sphere-like and rod-like MCAs. However, the different morphologies did not affect the heat release rate, total smoke release, average carbon monoxide yield, and average carbon dioxide yield based on the cone calorimeter. The flame-retardant mechanism of MCAs with different morphologies was investigated via thermal gravimetric analysis (TGA) and TGA-Fourier transform infrared spectra. The results show that the different morphologies of MCA resulted in different dispersed evenness of MCA. Further, the nanometer-scale flake-like morphology of MCA brought more interactions of hydrogen bond between MCA and PA6, which resulted in the delay of MCA decomposition and the enhancement of MCA flame-retardant effect. The nanometer-scale flake-like MCA had a better performance compared with the other samples because of the delaying and even release of flame-retardant effect by the decomposition of evenly dispersed MCA.
 J. Appl. Polym. Sci. **2014**, *131*, 40558.

KEYWORDS: flame-retardant; melamine cyanurate; morphology; PA6

Received 25 November 2013; accepted 4 February 2014
DOI: 10.1002/app.40558

INTRODUCTION

Polyamide 6 (PA6) is an important engineering plastic because of its good physical–mechanical properties, attrition resistance, and oil resistance. PA6 is widely employed in modern industrial applications.[1–3] Although PA6 possesses a limiting oxygen index (LOI) value of 24% and a UL94 V-2 rating, its flame retardancy should still be improved to meet the flame-retardant requirements of its application in several areas.[4–6] Therefore, inorganic flame-retardants melamine cyanurate (MCA),[5] organic alkyl phosphate,[7] and brominated polystyrene have all been incorporated to flame-retardant PA6.[8]

Similar to fillers,[9] inorganic flame retardants have to be added in greater amounts to achieve a satisfactory flame-retardant performance. These flame retardants provide different effects on the comprehensive properties of the material because of their different morphologies and surface properties.[10–13] In recent years, flame retardants with particular morphologies have been reported, such as $4ZnO{\cdot}B_2O_3{\cdot}H_2O$ with nanostructures,[14,15] nano-magnesium hydroxide,[9] and $NaAl(OH)_2CO_3$ whiskers.[16] Particular flame retardants enhance the char yield,[14,15] delay the time to ignition,[9] decrease the mean heat release rate (HRR),[9] or increase the mechanical reinforcement of the material.[16] Namely, several flame retardants with different morphologies show distinct advantages in enhancing the flame-retardant properties compared with the others.[9,14–16] Thus, morphology optimization has increasingly become an alternative way to improve the flame retardancy of additives.

MCA has been widely utilized as an important halogen-free flame retardant in unfilled polyamides.[17] As an inorganic flame retardant, MCA also needs to be incorporated in PA6 by approximately 15 wt % to obtain a flame retardant PA6 with UL94 V-0 rating.[18–20] A high addition level usually causes a negative effect on the properties of PA6, but MCA can be controlled and prepared to obtain several products with different morphologies. This condition may result in different effects on the flame retardancy and mechanical properties of MCA. Therefore, our recent research focuses more on the relationship between their morphologies and properties.

Table I. Formulations of the Flame-Retardant PA6 Compositions

Samples	PA6 (wt %)	MCA-A (wt %)	MCA-B (wt %)	MCA-C (wt %)
PA6	100	-	-	-
MCA-A/PA6	92	8	-	-
MCA-B/PA6	92	-	8	-
MCA-C/PA6	92	-	-	8

In this study, MCA particles with different morphologies (i.e., rod-like, sphere-like, and flake-like) were synthesized and applied in PA6. The effects of MCA morphologies on the flame-retardant properties of MCA/PA6 composites were also investigated.

EXPERIMENTAL

Materials

Melamine (99.0%, industrial products) and cyanuric acid (98.5%, industrial products) were supplied by Jinan Taixing Fine Chemical Co., Ltd. PA6 (melt index of 15.49 g/10 min) was obtained from Shijiazhuang Petroleum & Chemical Corporation. Hydrochloric acid (concentration of 37.0 wt %, analytical reagent) was obtained from Beijing Chemical Reagent Co., Ltd.

Instrumentation

The X-ray diffraction (XRD) patterns were obtained using a PANalytical company X' Pert PRO MPD X-ray diffractometer. This device was equipped with a Cu Kα generator ($\lambda = 0.15418$ nm) with a scanning rate of 0.033°/20 s in the 2θ range of 5° to 80°.

The microcosmic morphologies of MCA with a conductive gold layer were observed using a FP 2032/14 Quanta 250 FEG scanning electron microscope (SEM) at high vacuum and at 20 kV.

Thermo gravimetric analysis (TGA) tests were carried out using a TA instrument Q5000 IR thermal gravimetric analyzer at a heating rate of 20°C/min from 50°C to 700°C in N2 atmosphere. The typical results from TGA were reproducible within ±5%, and the reported data were average value based on three measurements.

The LOI values were obtained using a Fire Testing Technology (FTT, UK) Dynisco LOI instrument according to ASTM D2863-97, and the sheet dimensions were 130 mm × 6.5 mm × 3.2 mm. Each specimen was repeated three times and their error value were in ±0.5%.

The vertical burning test (UL94) was performed using a FTT0082 instrument based on the ANSI/UL-94–2009 testing procedure, and the sheet dimensions were 126 mm × 12.7 mm × 3.2 mm.

Fire behavior was characterized using a FTT cone calorimeter based on ISO5660 at an external heat flux of 50 kW/m^2. The dimension of the samples was 100 mm × 100 mm × 4 mm. The Typical results from the cone calorimeter tests were reproducible within ±5%, and the reported parameters were the average from three measurements.

The Fourier transform infrared (FTIR) spectra were obtained from a Nicolet iN10MX type spectrometer with KBr pellets.

TGA-FTIR tests were performed on a NETZSCH TG 209 F1 that was interfaced with a Nicolet 6700 FTIR spectrophotometer. The sample was placed in an alumina crucible and heated from 40°C to 800°C, at a heating rate of 20°C/min in N_2 atmosphere.

Synthesis of Sphere-like MCA (MCA-A)

About 1700 mL of water was added into a 10-L jacketed reactor with a stirrer. The water temperature was then raised to 85°C. About 135 mL of hydrochloric acid was added into the reactor, and the temperature of the mixture was raised to 90°C. Next, 168 g (1.30 mol) of melamine was added and stirred until completely dissolved. About 172 g of cyanuric acid (1.30 mol) was added into the mixture. The mixture was stirred at 90°C for 2 h. The powdery products were filtered and washed by water until their pH value reached 7. The resulting MCA was dried at 140°C for 4 h. The MCA yields were 314.5 g.

Synthesis of Rod-like MCA (MCA-B)

About 4000 mL of water was added into a 10-L jacketed reactor equipped with a stirrer. The water temperature was then raised to 95°C. About 170 g (1.35 mol) of melamine was added into the water and stirred until completely dissolved. Next, 174 g (1.35 mol) of cyanuric acid was then added into the mixture. The mixture was stirred at 100°C for 2 h. The powdery products were collected from the water by

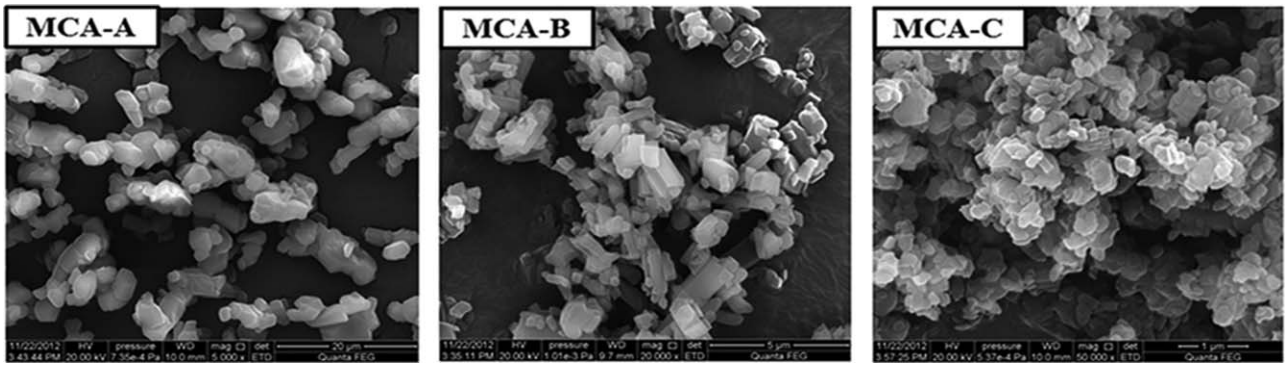

Figure 1. SEM photos of the MCA crystals.

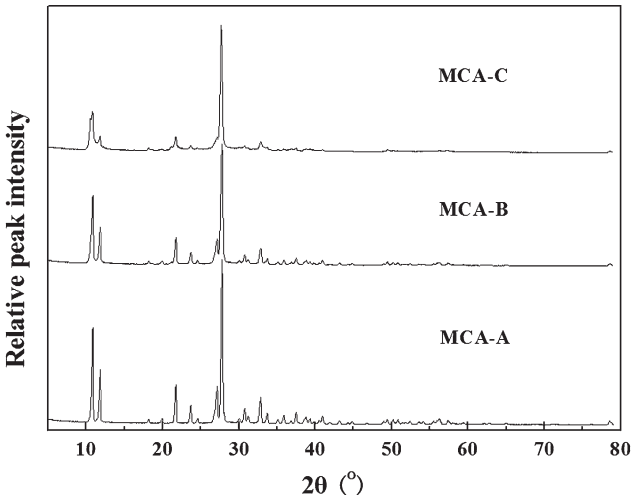

Figure 2. XRD patterns of the three types of MCAs.

filtering and dried at 140°C for 4 h. The MCA yields were 334.7 g.

Synthesis of Flake-like MCA (MCA-C)

About 2400 mL of water was added into a 10-L jacketed reactor equipped with a stirrer. The water temperature was then raised to 75°C. About 302.4 g (2.40 mol) of crushed melamine and 309.6 g (2.40 mol) crushed cyanuric acid were added into the reactor at the same time. The mixture was then stirred at 80°C for 2 h. The powdery products were filtered and dried at 140°C for 4 h. The products were smashed in a shredder, and their yields were 596.7 g.

Preparation of the Flame-Retardant PA6 Samples

The total content of MCA in PA6 was 8 wt %. The formulations of the flame-retardant PA6 composites are listed in Table I. All the composites were prepared using a twin extruder in the following conditions: the temperatures of sections 1–5 were 220°C, 230°C, 240°C, 230°C, and 225°C; the handpiece temperature was 220°C; and the screw speed was 8.6 r/s. The extruded strands were pelletized continuously after being cooled in a water bath. The pellets were dried at 90°C for 12 h. The composite pellets were then melted and injected into the standard models to prepare specimens for the flame-retardant and physical–mechanical property tests. The following injection conditions were set: plasticizing temperature of 230°C; storing pressure of 70 bar; storing flow of 60%; injection pressure of 40 bar; and injection flow of 25%.

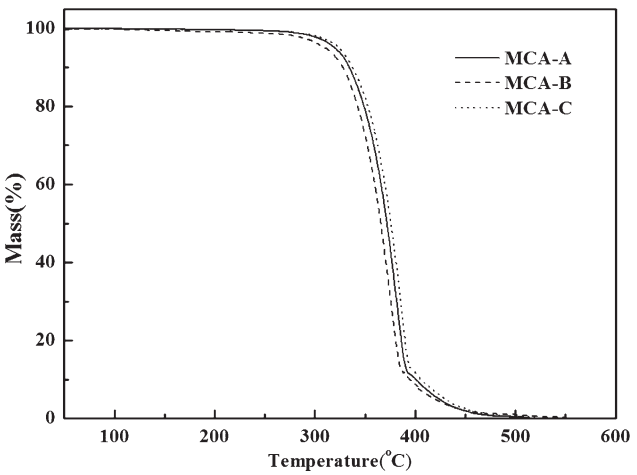

Figure 3. TGA curves of the three types of MCAs.

Table II. Results of the LOI and UL94 Tests on the Flame-Retardant MCA/PA6 Composites

Samples	PA6	MCA-A/PA6	MCA-B/PA6	MCA-C/PA6
LOI (%)	24.5	27.4	28.9	29.5
UL 94 rating	V-2	V-2	V-0	V-0

RESULTS AND DISCUSSION

Microcosmic Morphology of MCA

The SEM was carried out to evaluate the microcosmic morphologies of MCA particles. Their microcosmic photos are shown in Figure 1. The shape of the MCA-A particles is irregular sphere, whose diameters are approximately 5–10 μm. The shape of the MCA-B particles is mainly rod-like crystals (5 μm length, 1 μm width) and mixed with some irregular crystal fragments produced by grinding. The crystal shape of the MCA-C particles is nanometer-scale flake, whose diameters are approximately 200–300 nm and whose thickness are approximately 30–40 nm.

Based on the chemical structure of MCA, its morphology tends to form planar flakes. But in fact, MCAs with different morphologies were prepared in the experiments because the reaction process is easily influenced by the reaction conditions. These conditions include reaction temperature, pH value, reactant concentration, and the diameters of the reactant particles. The post process is also an important factor that affects the morphology of MCA. The irregular sphere-like MCA-A was obtained in an acid reaction condition because the melamine molecule could be induced by H cations, which led to the activation of amino groups in melamine molecules and promoted crystal growth in almost all directions. Accordingly, the MCA crystal of irregular sphere-like morphology was formed. Compared with the other two specimens, the rod-like MCA-B was obtained at a higher reaction temperature and a lower concentration of reactants, thereby contributing to the formation of longer crystals. Based on further tests, longer crystals were

Table III. Cone Calorimeter Data of Each Flame-Retardant MCA/PA6 Composites

Samples	PA6	MCA-A/PA6	MCA-B/PA6	MCA-C/PA6
Peak HRR (kW/m^2)	1059.6	923.9	854.8	883.7
THR (MJ/m^2)	120.2	117.2	111.8	113.6
av-COY (kg/kg)	0.032	0.027	0.033	0.029
av-CO_2Y (kg/kg)	2.42	2.15	2.23	2.41
TTI (s)	74	65	60	61
TSR (m^2/m^2)	502.5	595.1	577.8	589.5

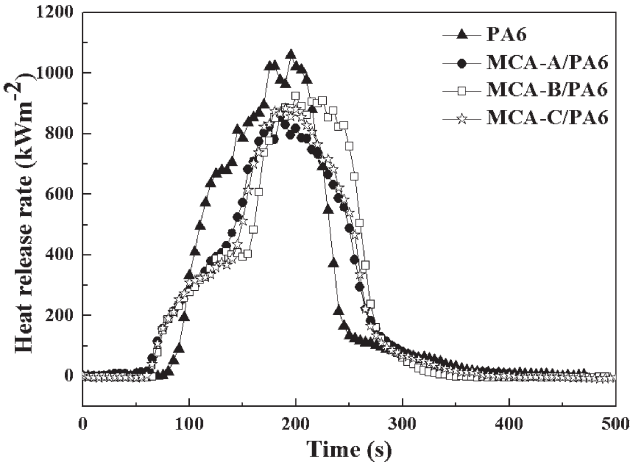

Figure 4. HRR curves of the MCA/PA6 composites.

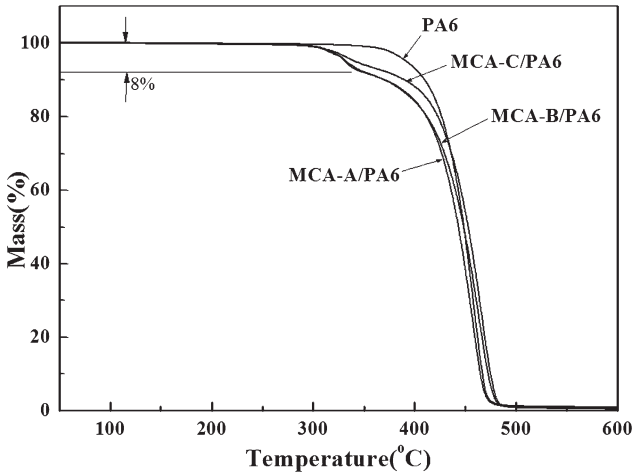

Figure 5. TGA curves of the PA6 and MCA/PA6 composites.

obtained when higher reaction temperatures were employed at low concentrations of reactants. By contrast, nano-flake MCA-C was prepared at a higher concentration of reactants and a lower reaction temperature. This condition can reduce the solubility of MCA in solutions and promote the earlier formation of small MCA crystals. Besides, the post process also caused breaking of the few longer flake-like MCA crystals, thereby ensuring a uniform MCA-C morphology.

XRD Analysis of the MCA Particles

Figure 2 shows the XRD patterns of the three types of MCA samples. Their main peaks, including 10.8°, 11.8°, 21.8°, 27.7°, and 32.9°, are similar in position, which indicate a fundamentally identical crystal structure of MCAs. However, the differences between their peak intensities show that the crystals have different growth scales in different directions and thus possess various macrocosmic particle sizes. The MCA-A pattern shows smaller peaks aside from the main peaks compared with the three XRD patterns of the MCA samples. This observation implies that the crystal cell of MCA-A has a more irregular arrangement that leads to irregular spherical particles. The MCA-B pattern exhibits fewer peaks than MCA-A but more than MCA-C. Accordingly, MCA-B has a relatively regular crystal shape but with uneven sizes. The MCA-C pattern is the simplest among all three samples. Thus, its crystal shape and size are also the most uniform. The XRD result of MCA-C is consistent with the microcosmic morphology in the SEM image. All the results were caused by their reaction conditions. As previously discussed, the acid imposed a strong effect on the formation of MCA-A crystals because of the hydrogen bond action of the H cations. The high reaction temperature activated hydrogen ions from water dissociation and thus affected the formation of MCA-B. A high concentration of the reactants and a low reaction temperature brought the least disturbance to the formation of small MCA-C crystal. Therefore, the different reaction conditions led to the morphology changes of growing crystal.

TGA Analysis of MCAs

The thermo weight loss behaviors of the three types of MCAs are shown in Figure 3. The decomposition process of MCA started at nearly 310°C and terminated at nearly 500°C. The remaining mass of all the specimens at 550°C was almost 0%. These data indicate that MCA had a high thermal stability, which enables it to meet the temperature required in the processing of most polymers. MCA was also completely decomposed without residual char, which reveals its flame-retardant effect in gaseous phase rather than in condensed phase. More importantly, the three TGA curves of the MCAs with different morphologies had similar decomposition routes. This result implies that the different microscopic morphologies of MCA do not influence its thermal degradation behavior because such behavior is usually related to the stability of the chemical bonds in the compound and not to their morphologies.

LOI and UL94 Vertical Burning Tests

LOI and UL 94 vertical burning tests were carried out to investigate the flame-retardant performance of MCAs with different morphologies on PA6. The results are summarized in Table II. The pure PA6 sample only obtained an LOI value of 24.5% and

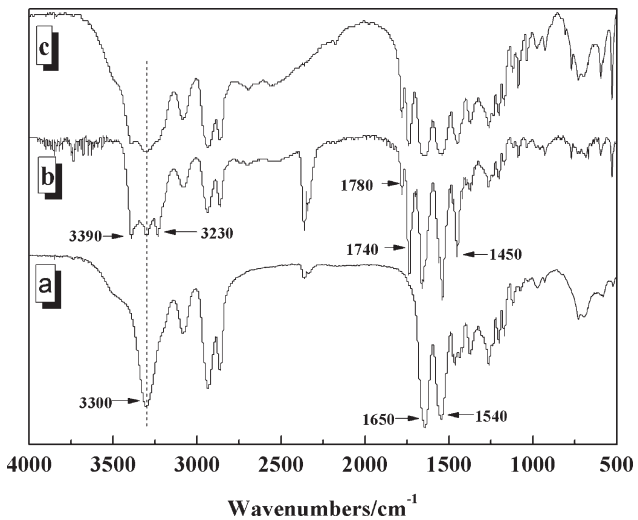

Figure 6. The FTIR spectra of (a) neat PA6, (b) the control mixture of 8% MCA-C and 92% PA6 powders without melting process, and (c) the MCA-C/PA6 composites.

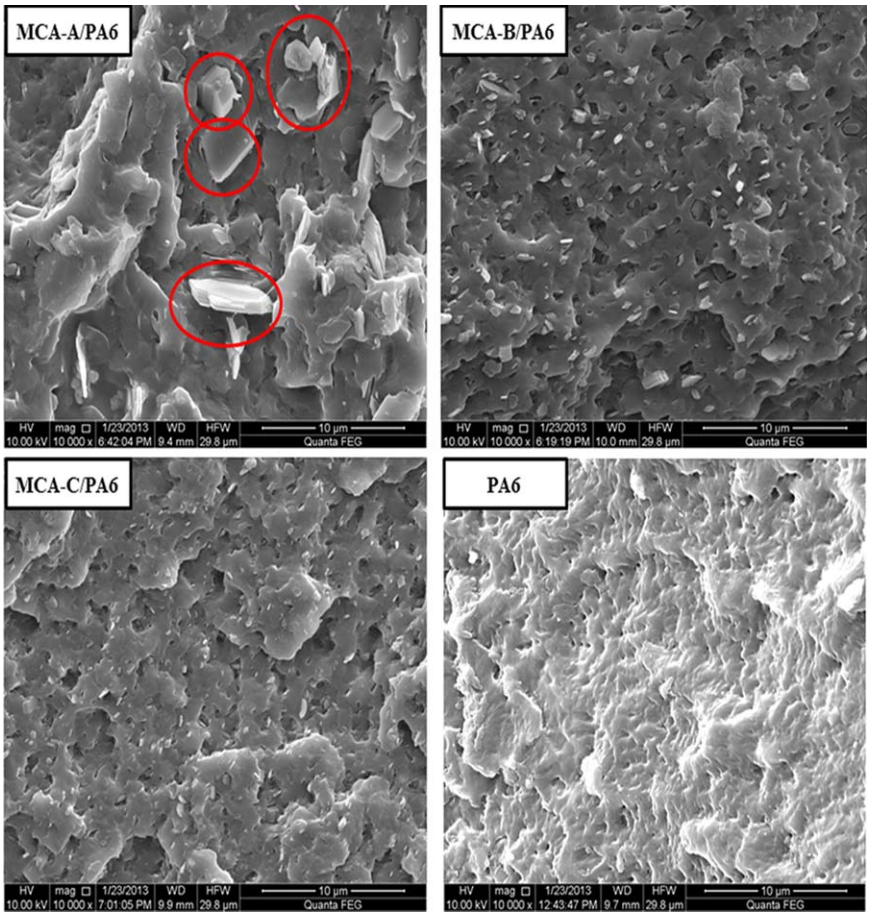

Figure 7. SEM photos of the fracture surfaces of the MCA/PA6 composites. [Color figure can be viewed in the online issue, which is available at wileyonlinelibrary.com.]

reached a UL 94 V-2 rating. After the three types of MCA particles were incorporated into PA6, the flame-retardant properties of each MCA/PA6 sample were all enhanced, respectively. Although these MCAs were only different in morphology, the flame-retardant properties of the composites brought by MCAs still revealed obvious variations. The addition of MCA-C, whose size is the smallest among the three specimens, resulted in the maximum LOI value, although the contents of MCAs with different morphologies in the composites were the same. The UL94 test results also showed a different effect caused by morphology. The composites with 8 wt % MCA-B and MCA-C reached a UL94 V-0 rating, but that with 8 wt % MCA-A still had a UL94 V-2 rating. After comparing all the data, the flame retardancy sequence of MCA was determined to be MCA-C > MCA-B > MCA-A, and the size of the MCA particles has a significant effect on their flame retardancy. The results can be explained that MCA with a smaller size dispersed more evenly in the microcosmic PA6 matrix, which exerted a more continuous flame-retardant effect when the MCA/PA6 composites were ignited.[9]

Cone Calorimeter Test

The cone calorimeter data of the MCA/PA6 composites are summarized in Table III, and the HRR curves are shown in Figure 4. When the MCAs were incorporated into PA6, the peak of HRR and total heat release (THR) of the MCA/PA6 composites slightly decreased by less than 20%. Moreover, the total smoke release (TSR) of the MCA/PA6 composites increased by less than 20%. The time to ignition (TTI) of the MCA/PA6 composites also increased by approximately 9 s to 13 s. The average CO yields (av-COY) and average CO_2 yields (av-CO_2Y) had no evident changes. All the results from the cone calorimeter tests of the three types of MCA/PA6 composites were fundamentally consistent. These results imply that the morphologies of MCA do not cause a significant effect on the burning process of the MCA/PA6 composites. The above results only illustrate that the different-morphology MCAs displayed the same flame-retardant effect. During the combustion of the MCA/PA6 composites, MCA was decomposed earlier than PA6 matrix, and the decomposition of MCA absorbed some combustion heat and released non-flammable gases that diluted O_2 and flammable gas.[19] After MCA was completely decomposed, the decomposed products from PA6 still burned. The incorporated MCA only decreased the amount of flammable PA6 matrix.

TGA Analysis of the MCA/PA6 Composites

The TGA curves of PA6 and MCA/PA6 composites are shown in Figure 5. The MCA/PA6 composites started to lose mass at 300°C, which is equal to the onset decomposition temperature of MCA but lower than that of PA6. As shown in Figure 5, the

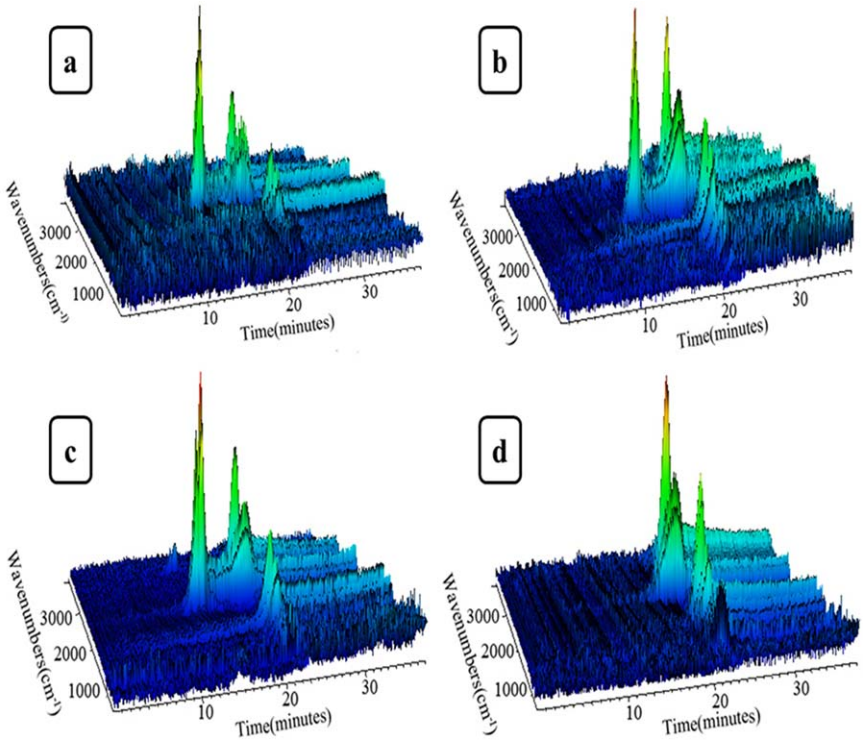

Figure 8. 3D FTIR spectra of the TGA gaseous products of the samples. (a) MCA-A/PA6, (b) MCA-B/PA6, (c) MCA-C/PA6, and (d) PA6. [Color figure can be viewed in the online issue, which is available at wileyonlinelibrary.com.]

mass loss ratio of MCA/PA6 is exactly 8 wt %, which is equal to the MCA contents in the MCA/PA6 composites. This result proves that MCA almost completely decomposed before the start of the PA6 decomposition. At 700°C, the residual weight values of the MCA/PA6 and PA6 samples were almost 0 wt %, which indicates that all MCAs with different morphologies had no effect on the increasing residue weight. In addition, the mass loss of MCA-C/PA6 occurred at approximately 370°C, which is lower than that of the other two MCA/PA6 samples. The delay was caused by the formation of more hydrogen bonds between MCA nanometer-scale flakes and the PA6 matrix in their interface, which can be verified in the subsequent discussion. More hydrogen bonds promoted the increase in the thermal stability of MCA and led to the decomposition temperature of MCA close to that of the PA6 molecule. PA6 molecules are known to have plenty of acylamino groups, whereas MCA molecules possess carbonyl, amino, and hydroxyl groups. When MCA particles become smaller or even reach the nanometer scale, many groups on the MCA particle surface will react with the carbonyl groups in PA6, which results in the formation of more hydrogen bonds between MCA and PA6 molecules. Therefore, nanometer-scale MCA may combine with the PA6 matrix to become more stable, thereby promoting the compatibility of MCA and PA6 matrix.

The formation of hydrogen bonds can be verified by the FTIR spectra of composites as shown in Figure 6. Figure 6 shows the FTIR spectra of neat PA6 [Figure 6(a)], the control mixture of 8% MCA-C and 92% PA6 powders without melting process [Figure 6(b)], and the MCA-C/PA6 composite [Figure 6(c)]. In Figure 6(a), the peaks at 3300 cm^{-1} was ascribed to the vibrations of amino groups of PA6 molecule and the peaks at 1650 cm^{-1} and 1540 cm^{-1} were ascribed to the vibrations of carbonyl group of PA6 molecule. In Figure 6(b), the peaks at 3390 cm^{-1} and 3230 cm^{-1} were caused by the stretching vibrations of amino groups of MCA molecule, while the peaks at 1650 cm^{-1} and 1540 cm^{-1} were the superposition of the vibrations of carbonyl group in both MCA and PA6 molecules, and the vibration of triazine ring in MCA molecule may lead to the absorption peaks at 1780 cm^{-1} and 1740 cm^{-1}. Importantly, the intensity ratio of the peak at 1740 cm^{-1} to the peak at 1650 cm^{-1} in both Figure 6(b) and Figure 6(c) were identical, which implies that the mass fraction of MCA in samples were same in the mixed powders of Figure 6(b) and the MCA-C/PA6 composite of Figure 6(c). However, the notable change can be observed in Figure 6(c) compared with Figure 6(b). The typical absorption peaks especially the ones at 3390 cm^{-1}, 3230 cm^{-1}, 1650 cm^{-1}, and 1540 cm^{-1} representing acylamino group became smooth even vanished, which revealed the existence of hydrogen bond between MCA and PA6 molecules. The interactions of hydrogen bond may result in the change of electron atmosphere configuration and the assimilation of functional groups vibration in FTIR spectra.

The results of the UL94 and LOI tests can be easily understood using the above explanation. PA6 usually produces molten drip during combustion. The drip can remove heat and fire but may ignite the absorbent cotton under the specimen. Thus, PA6 has a UL94 V-2 rating. If the drip is inhibited from

igniting the cotton, the composites will attain a UL94 V-0 rating. MCA in PA6 can release heat sink and the inert gas to terminate the ignition process. However, the decomposition temperature of MCA is lower than the dripping of the PA6 matrix. The decrease in MCA size promoted the formation of more hydrogen bonds, which slightly raised the decomposition temperature of MCA. Therefore, the higher decomposition temperature of MCA was close to the decomposition temperature of PA6, which contributed MCA to exerting flame-retardant effect during PA6 decomposition. Namely, nanometer-scale MCA can extinguish the fire on the MCA/PA6 composites more effectively. That's why the smaller size of MCA can bring a better flame-retardant effect to the MCA/PA6 composites.

The Dispersion of MCAs in MCA/PA6 Composites

The dispersion of MCAs with different morphologies in PA6 was investigated via SEM to observe the fracture surface of the MCA/PA6 composites. The SEM photos are shown in Figure 7. The photo of a neat PA6 fracture surface only exhibits a wavy appearance. However, the photos of the MCA/PA6 fracture surface reveal that a large number of MCA particles evenly exist on these surfaces without aggregation, which are obviously different from that of neat PA6. The photos in Figure 7 confirm that the MCA particles all sustained their microcosmic particle morphologies that were not destroyed by shear and extrusion forces during processing. Smaller MCA particles were evenly dispersed in the matrix. The smaller particle size of the MCA particles also contributed to a more even decomposition and release of flame-retardant effect during the ignition of the MCA/PA6 composites.[9]

TGA-FTIR Analysis of the MCA/PA6 Composites

Figure 8 shows the FTIR spectra of the TGA gas products of the PA6 and MCA/PA6 samples with increasing temperature at a heating rate of 20°C/min. The main TGA gas peak of PA6 appears at approximately 18 min and 360°C and disappears at 24 min and 480°C. Compared with that of PA6, the MCA/PA6 FTIR spectra exhibited an additional single peak at approximately 15 min and 300°C, which corresponds to the decomposition temperature of MCA. Moreover, the peaks of the gaseous products from MCA were independent and did not result in any obvious peak changes from the pyrolysis gaseous products of the PA6 matrix. The independent release and no effect on the pyrolysis gaseous products of PA6 further confirmed that MCA only exerted flame-retardant effect in physical way, and the pyrolysis gaseous products of MCA only diluted the flammable gas to exert its flame-retardant purpose. Accordingly, the different morphologies of MCA do not affect the ignition behavior and decomposition route of the PA6 matrix and only change the evenness of MCA decomposition during combustion.

CONCLUSIONS

Three types of MCA particles with micrometer-scale rod-like, micrometer-scale sphere-like, and nanometer-scale flake-like morphologies, were synthesized by changing the chemical reaction conditions, respectively. The MCA/PA6 composites incorporated with different-morphology MCA particles showed different flame-retardant effects in LOI and UL94 rating tests. The nanometer-scale flake-like MCA brought an LOI value of 29.5% and a UL94 V-0 rating to MCA/PA6 composites, which were better than those of micrometer-scale sphere-like and rod-like MCAs. The results reveals that the nanometer-scale flake-like morphology of MCA brought more interactions of hydrogen bond between MCA and PA6, which resulted in the delay of MCA decomposition and the enhancement of MCA flame-retardant effect. The nanometer-scale MCA also obtained the better dispersion in PA6 matrix than the other MCA samples. Further, the better flame-retardant performance of nanometer-scale flake-like MCA is resulted by the delay of MCA decomposition and the more even release of the flame-retardant effect from the decomposed MCA.

ACKNOWLEDGMENTS

Financial support was provided by the Education Science & Research Development Project of Beijing Municipal Institutions (No. KM201110011010).

REFERENCES

1. Chen, J. S.; Liu, M.; Zhao, J. Q. *Polym. Degrad. Stab.* **2011**, *96*, 1508.
2. Tai, Q. L.; Richard, K. K.; Yang, W.; Qiao, Z. H.; Song, L.; Hu, Y. *Compos. A* **2012**, *43*, 415.
3. Wu, Z. Y.; Xu, W.; Xia, J. K.; Liu, Y. C.; Wu, Q. X.; Xu, W. J. *Chinese Chem. Lett.* **2008**, *19*, 241.
4. Zhang, J. P.; Michael, A. D.; Serge, B. *Combust. Flame* **2009**, *156*, 2056.
5. Chen, Y. H.; Wang, Q.; Yan, W.; Tang, H. M. *Polym. Degrad. Stab.* **2006**, *91*, 2632.
6. Zhu, S. F.; Shi, M. W.; Zhu, M. F. *Mater. Lett.* **2013**, *99*, 28.
7. Hu, Z.; Chen, L.; Lin, G. P.; Luo, Y.; Wang, Y. Z. *Polym. Degrad. Stab.* **2011**, *96*, 1538.
8. Horrocks, A. R.; Smart, G.; Kandola, B.; Price, D. *Polym. Degrad. Stab.* **2012**, *97*, 645.
9. Gui, H.; Zhang, X. H.; Liu, Y. Q.; Dong, W. F.; Wang, Q. G.; Gao, J. M.; Song, Z. H.; Lai, J. M.; Qiao, J. L. *Compos. Sci. Technol.* **2007**, *67*, 974.
10. Takashi, K.; Richard, H. H. J.; Zhang, X.; Briber, R. M.; Bani, H. C.; Srinivasa, R. R.; Walid, H. A.; John, R. S. *Polymer* **2004**, *45*, 881.
11. Modesti, M.; Lorenzetti, A.; Besco, S.; Hrelja, D.; Semenzato, S.; Bertani, R.; Michelin, R. A. *Polym. Degrad. Stab.* **2008**, *93*, 2166.
12. Nizar, D.; Stéphane, G.; Eric, D.; Guillaume, L. *Polym. Degrad. Stab.* **2012**, *97*, 383.
13. Jin, D. L.; Gu, X. Y.; Yu, X. J.; Ding, G. S.; Zhu, H. L.; Yao, K. H. *Mater. Chem. Phys.* **2008**, *112*, 962.
14. Zhang, Y. Y.; Li, P.; Liu, Z. H. *Powder Technol.* **2011**, *210*, 208.

15. Zhang, Y. Y.; Xue, L.; Liu, Z. H. *Thermochim. Acta* **2010**, *506*, 52.
16. Li, X.; Ye, J. W.; Lin, Y.; Fan, L. L.; Pang, H. C.; Gong, W. T.; Ning, G. L. *Powder Technol.* **2011**, *206*, 358.
17. Casu, A.; Camino, G.; Giorgi, M. D.; Flath, D.; Morone, V.; Zenoni, R. *Polym. Degrad. Stab.* **1997**, *58*, 297.
18. Dogan, M.; Yılmaz, A.; Bayramlı, E. *Polym. Adv. Technol.* **2011**, *22*, 560.
19. Gijsmana, P.; Steenbakkersa, R.; Fürstb, C.; Kersjesc, J. *Polym. Degrad. Stab.* **2002**, *78*, 219.
20. Kiliaris, P.; Papaspyrides, C. D. *Prog. Polym. Sci.* **2010**, *35*, 902.